



# VCU

Virginia Commonwealth University  
VCU Scholars Compass

---

Theses and Dissertations

Graduate School


---

2016

## Characterization of Poly(dimethylsiloxane) Blends and Fabrication of Soft Micropillar Arrays for Force Detection

Thomas J. Petet Jr  
*Virginia Commonwealth University*

Follow this and additional works at: <https://scholarscompass.vcu.edu/etd>

 Part of the [Biomaterials Commons](#), [Biomechanics and Biotransport Commons](#), and the [Molecular, Cellular, and Tissue Engineering Commons](#)

© Thomas John Petet Jr.

---

Downloaded from

<https://scholarscompass.vcu.edu/etd/4649>

This Thesis is brought to you for free and open access by the Graduate School at VCU Scholars Compass. It has been accepted for inclusion in Theses and Dissertations by an authorized administrator of VCU Scholars Compass. For more information, please contact [libcompass@vcu.edu](mailto:libcompass@vcu.edu).

© Thomas John Petet Jr. 2016  
All Rights Reserved

**Characterization of Poly(dimethylsiloxane) Blends and Fabrication of Soft Micropillar  
Arrays for Force Detection**

A thesis submitted in partial fulfillment of the requirement for the degree of Masters in  
Biomedical Engineering at Virginia Commonwealth University.

by

Thomas John Petet Jr.  
Biomedical Engineering B.S, Virginia Commonwealth University, 2014

Director: Dr. Christopher Lemmon, Ph.D.  
Assistant Professor, Biomedical Engineering

Virginia Commonwealth University  
Richmond, Virginia  
October 2016

## Acknowledgements

Thanks Mom and Dad for forcing me into college. I quite literally would not be where I am today without all the pushing, prodding, encouraging, and support I have been blessed with over the years. Thanks Rachel for forcing me to think critically and being that person I can go to for support with pretty much anything outside of biomechanics. I wouldn't push that onto you. Thanks Dr. Lemmon for teaching me skills and taking a chance on me. You have put your neck on the line many times for me, even when I was a less than stellar student. Thanks to all my professors for only failing me a little bit and teaching me quite a lot. All the support the Lemmon lab showed during the good and bad times really helped me grow into the person I am now.

<b>Table of Contents</b>	<b>Page</b>
List of Tables	iv
List of Figures	v
List of Abbreviations	vi
List of Equations	vii
Abstract	viii
Chapter 1: Introduction and Background	1
Chapter 2: Methods	6
Chapter 3: Results	21
Chapter 4: Discussion	38
Chapter 5: Conclusions and Future Directions	42
References	44
Curriculum Vita (CV)	48

**List of Tables****Page**

Table 1: Mixing Weights for 184 Ratios

7

Table 2: Mixing Weights for 184:527 Blends

8

<b>List of Figures</b>	<b>Page</b>
Figure 1: Molecular Structure of PDMS	9
Figure 2: Basic Diagram of Rheometry Process	10
Figure 3: Diagram of Dog Bone with Approximate Dimensions	11
Figure 4: Autodesk Inventor Model of Posts	14
Figure 5: Post Rinse Diagram	17
Figure 6: Complex Shear Modulus Values for All PDMS Polymers	22
Figure 7: Complex Shear Modulus as a Function of Polymer Percent Composition	23
Figure 8: Important PDMS Complex Shear Modulus Values	24
Figure 9: Elastic Modulus Data of Important PDMS Polymers	25
Figure 10: Representative Cell Images from Polymer Attachment Assay	27
Figure 11: Polymer Attachment Assay Results	29
Figure 12: Autodesk Inventor Strain Model	31
Figure 13: Post Imaging Strategy Diagram	32
Figure 14: #7 Posts, 3:1 PDMS Blend Example Image	33
Figure 15: #5 Posts, 1:1 PDMS Blend Example of Collapsed Posts	34
Figure 16: Post Force Data	36

## List of Abbreviations

PDMS – Poly(dimethylsiloxane)

184 PDMS – PDMS with 184 monomer units

527 PDMS –PDMS with 527 monomer units

184 Ratio – Polymers that use only ratios of 184 PDMS

184:527 Blend – Polymers that use only ratios of 184 PDMS mixed at 10:1 and 527 PDMS mixed at 1:1

Fn – Fibronectin

BSA – Bovine Serum Albumin

EMT – Epithelial to Mesenchymal Transition

#5 – 5  $\mu\text{m}$  tall posts

#7 – 7  $\mu\text{m}$  tall posts



## List of Equations

$$1) \delta = F \left( \frac{4L^3}{3\pi E r^4} \right)$$

$$2) k = \frac{3\pi E r^4}{4L^3}$$

$$3) F = k\delta$$

$$4) G = \sqrt{G_E^2 - G_V^2}$$

$$5) E = 2G(1 + \gamma)$$

## Abstract

Diseases involving fibrosis cause tens of thousands of deaths per year in the US alone. These diseases are characterized by a large amount of extracellular matrix, causing stiff abnormal tissues that may not function correctly. To take steps towards curing these diseases, a fundamental understanding of how cells interact with their substrate and how mechanical forces alter signaling pathways is vital. Studying the mechanobiology of cells and the interaction between a cell and its extracellular matrix can help explain the mechanisms behind stem cell differentiation, cell migration, and metastasis. Due to the correlation between force, extracellular matrix assembly, and substrate stiffness, it is vital to make *in vitro* models that more accurately simulate biological stiffness as well as measure the amount of force and extracellular matrix assembly. To accomplish this, blends of two types of poly(dimethylsiloxane) (PDMS) were made and the material properties of these polymer blends were characterized. A field of 5 $\mu\text{m}$  or 7 $\mu\text{m}$  microscopic pillars (referred to as posts) with a diameter of 2.2 $\mu\text{m}$  were fabricated from these blends. Each combination of PDMS blend and post height were calibrated and the stiffness was recorded. Additionally, polymer attachment experiments were run to ensure cells survived and had a normal phenotype on the different blends of PDMS when compared to pure PDMS. Finally, cells were placed onto a field of posts and their forces were calculated using the new stiffness found for each blend of post. Varying the PDMS material stiffness using blends allow posts to be much more physiologically relevant and help to create more accurate *in vitro* models while still allowing easy and accurate force measurement. More biologically relevant *in vitro* models can help us acquire more accurate results when testing new drugs or examining new signaling pathways.

## Chapter 1: Introduction and Background

Worldwide, fibrotic diseases claim tens of thousands of lives every year. In the U.S. alone, about 45% of deaths are attributed to some form of fibrosis [1]. Fibrosis and regular wound healing share many signaling pathways [2]. Cytokines, integrin receptors, and mechanical feedback are all required for normal wound healing and under healthy conditions are highly regulated. When these pathways begin to lose that regulation, a large amount of scar tissue is deposited within the tissue. Many factors can cause fibrosis, but the effects are the same across tissue types. Large amounts of extracellular matrix proteins are assembled, increasing tissue stiffness and preventing complex tissue functions from being performed. Idiopathic pulmonary fibrosis (IPF) is an example of lost tissue functionality due to fibrosis. This disease is common disease in elderly adults and usually is lethal due excess extracellular matrix assembly blocking oxygen transport and raising the tissue stiffness, lowering lung compliance [3]. Medical costs directly related to treating IPF averaged about \$22,000 per patient in the year 2011 [4]. Some forms of fibrosis, such as scars formed on the skin, are not lethal but can lead to psychological issues. Many individuals who have large scars from surgery or other trauma tended to have lower self-confidence, anxiety, anger issues, and tended to be more depressed [5]. Fibrosis is the cause of not only serious health issues, but also a large financial burden on patients. A better understanding of the causes of fibrosis can help shed light on future treatments, lowering the mortality and cost of fibrosis related diseases.

To fully understand fibrosis, the extracellular matrix and substrate stiffness must first be examined. Extracellular matrix proteins are numerous and vary from tissue to tissue. Interactions between different proteins such as collagen, elastin, and fibronectin dictate the tissue's mechanical properties, as well as provide a scaffold for the cells to attach to [6]. Increased

amounts of extracellular matrix assembled causes an increase in substrate stiffness [7]. Changing vastly between tissue types, this scaffold can change cells' actions based on the different substrate stiffness alone. For example, human mesenchymal stem cells (HMSCs) given the same chemical signals can change what they differentiate into based on the substrate stiffness. Stiffer substrates drive differentiation of HMSCs towards bone, while softer substrates drive differentiation towards adipose cells [8]. Fibroblasts also can change their phenotype based on substrate stiffness. Substrate stiffness can permit fibroblasts to form "mature" focal adhesions, which are the proteins that connect the cells to the extracellular matrix. These mature focal adhesions are significantly larger than normal focal adhesions, allowing for greater cellular forces to be generated. This also allows  $\alpha$ -smooth muscle actin to be incorporated into the fibroblast's existing  $\beta$ -cytoplasmic actin, initializing a cascade of mechanical signals leading to differentiation to myofibroblasts [9], [10]. Substrate stiffness is vital to normal tissue functionality and is closely connected to cellular forces. As cellular force increases, the amount of extracellular matrix assembly increases, causing tissue stiffness to increase as well [11]. A controlled balance between cellular forces and substrate stiffness keep normal tissues from over assembling extracellular matrix fibers and forming large scars in tissues. Normal wound healing requires an amount of matrix assembly, but when cellular forces are not regulated matrix assembly increases without regulation, causing fibrosis [2], [12], [13]. Due to the fact that fibrotic diseases are characterized by large amounts of extracellular matrix assembly and an increase in stiffness in the affected area [13],[14], and assembly of the extracellular matrix is regulated largely by the amount of force a cell exerts [11], [15]–[18], better methods of characterizing cellular forces will lead to a better understanding of the mechanisms behind

fibrosis. Using an understanding of mechanobiology, the complex interactions between chemical and mechanical signaling can be used to either prevent or treat these diseases.

From the evidence above, a key in understanding fibrotic diseases lies with understanding how changing substrate stiffness effects cellular forces that control extracellular matrix assembly. Quantifying the amount of assembly of the extracellular matrix as stiffness changes is easily accomplished via immunofluorescent staining and image processing. To examine more closely the effects of substrate stiffness on extracellular matrix assembly, many artificial substrates have been made to precisely control the stiffness that a cell experiences. Glass coverslips are commonly used in *in vitro* applications. Though this allows easy extracellular matrix examination, glass has an elastic modulus of  $\sim 3$  GPa, while soft tissues are typically between 0.4 kPa and 20 kPa. As such, glass is not soft enough to model a physiologically relevant substrate stiffness. To get closer to physiological levels, coating a coverslip with a polymer such as PDMS drastically softens the surface depending on the ratio of PDMS used. Another method of creating a physiologically relevant substrate involves creating a polyacrylamide based hydrogel. This stiffness can be controlled by altering the ratio of acrylamide to bis-acrylamide before polymerizing with ammonium persulfate [19].

Measuring cellular forces is a much more complicated process. One approach to measuring cell forces is called traction force microscopy (TFM) in which one uses fluorescent beads mixed into a PDMS or polyacrylamide gel surface. This method consists of seeding cells onto this sheet, imaging the cells on the gel as well as the fluorescent beads, then lifting the cells off the surface of the gel and imaging the new “relaxed” position of the fluorescent beads. Though the signal to noise ratio is much more favorable in this protocol and the data much easier to acquire, some assumptions must be made that may not be true. Analysis of forces on these

substrates is difficult, as the data only includes deflection of points in the gel, without discrete knowledge of where forces are applied. Solving for forces requires the application of boundary conditions that strongly influence the calculated forces [20]–[22].

Another way to measure the forces that cells exert onto their substrate are micropillar arrays, also referred to as microfabricated posts [23]. By seeding cells onto the tops of the posts, the forces generated by cells can be calculated by using the simple stress-strain mechanics of a cantilever beam with a point force at the free end. This eliminates the issues that arise from the fluorescent gel force measurement system, however it causes problems in two ways. First, it has been argued that the cells on the posts do not act normally due to the large gaps between the points where the cells contact the posts. Unlike in physiological conditions, posts are a set of discrete points and not a homogeneous surface. This can be addressed through proper treatment of the posts (explained in the methods section). The second issue with posts involves the amount of deflection the posts undergo due to the force of cells. As shown in equation 1, deflection ( $\delta$ ) is dependent on the geometry of the post. Ease of fabrication depends on the geometry as well. Taller posts are more difficult to fabricate, but are easier for cells to bend. Because fabrication of the posts can be difficult as the height of the posts increases, using shorter posts is much more common. Cells may have a harder time generating enough force to cause a detectable deflection however, so there is a concern with the signal to noise ratio of the posts [22],[24]. The substrate stiffness of shorter posts is also greater than many tissues, causing the cells to experience an unrealistic amount of substrate stiffness. Upon investigating the current issues with posts, it was hypothesized that a change in the material properties of PDMS by blending a stiff and a soft polymer together would generate posts that not only gave more sensitive force measurements, but also more closely modeled the stiffness of biological tissues.

In order to control the stiffness and measure cellular forces, microscopic pillars made of PDMS (posts) can be used [23]. Posts provide a way to modulate the effective stiffness that a cell experiences by changing the height and radius of each pillar. Stiffness ( $k$ ) is calculated using the elastic modulus ( $E$ ), radius ( $r$ ), and height ( $L$ ) of the posts in equation 2 . Their geometry can be precisely changed allowing the substrate stiffness to go down as the height of the posts increase or radius decreases. Previously fabricated posts allow for both softer stiffness values to be attained, as well as force measurements to be obtained from the displacement of the posts due to cell interactions. Posts are regularly fabricated using a 10:1 ratio of PDMS base to cross-linker with a height of between  $5\mu\text{m}$  and  $15\mu\text{m}$  (5.8 kPa – 0.6 kPa). A limitation with post fabrication comes from attempts to generate taller, softer posts. Many of the posts taller than  $7\mu\text{m}$  tall (3.0 kPa) collapse during fabrication. Lowering the stiffness of posts to more physiologically relevant can only be accomplished by changing the geometry of the posts or using a polymer with a lower elastic modulus [23]. Using blends of two PDMS formulations, posts that are  $7\mu\text{m}$  tall can have an effective modulus of 1.2 kPa. Though still stiffer than some tissues, this stiffness range is well within many soft tissue stiffness values (between 0.9 kPa and 4.5 kPa), as well as endothelial tissue (1.5 kPa) and fibroblast (2.8 kPa) elastic moduli values [13].

## Chapter 2: Methods

### Selecting and Mixing PDMS Blends

To create the polymers for all the following experiments, Sylgard 184 PDMS and Sylgard 527 PDMS were prepared per recommended protocol (10:1 polymer to cross linker and 1:1 polymer to cross linker, respectively). After desiccation for 15-30 minutes to remove air bubbles, the two “pure” PDMS polymers were mixed to create a blend of 184 and 527 PDMS at different ratios. After mixing, the polymers were allowed another 15-30 minutes in the desiccator to remove all air bubbles once again. Curing temperatures of the PDMS varied depending on the application required. For any material testing, the PDMS was cured at 55 °C, while posts were cured at 110 °C. The exact measurements for each polymer blend can be seen below in tables 1 and 2 and the molecular structure of PDMS can be seen in Figure 1. [4]

### Material Testing

Characterization of the material properties of the PDMS blends consisted of two tests. Samples for both rheometry and tensile testing could be created at the same time by pouring 50g of each polymer into a P150 culture dish. Samples were then cut using a 20mm leather punch for rheometry or a scalpel for tensile testing. Three tensile samples and between 3 and 6 rheometry samples could be generated from one P150. Rheometry samples were centered on a DHR Rheometer from TA Instruments set up for a small amplitude oscillatory shear test and a frequency sweep test 100 – 1 Hz was run. For tensile testing, a speed of 10 mm/min was used to test the sample, with a total crosshead displacement of 6 mm. Figures 2 and 3 show the experimental setup for rheometry and dog bone shape sample for tensile testing, respectively.



<b>Blend</b>	<b>184 Base (g)</b>	<b>184 Crosslinker (g)</b>
<b>5:1</b>	50	10
<b>10:1</b>	50	5
<b>20:1</b>	60	3
<b>30:1</b>	60	2
<b>50:1</b>	50	1

Table 1: Mixing Weights for 184 Ratios

<b>Blend</b>	<b>184 10:1 (g)</b>	<b>527 1:1 (g)</b>
<b>3:1</b>	36	12
<b>2:1</b>	40	20
<b>1:1</b>	25	25
<b>1:2</b>	20	40
<b>1:3</b>	12	36

Table 2: Mixing Weights for 184:527 Blends

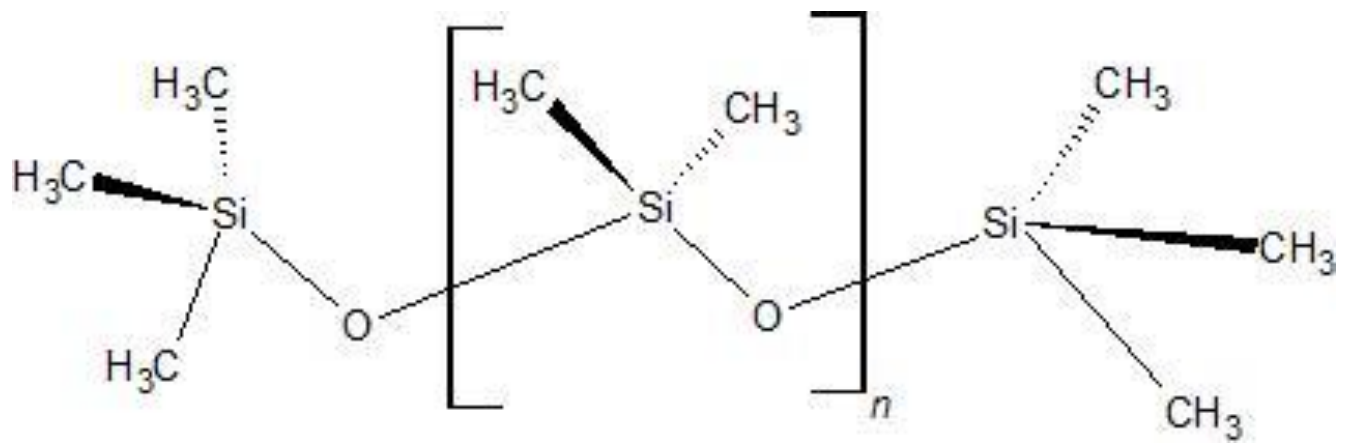


Figure 1: Molecular Structure of PDMS. The number associated with the PDMS polymer refers to the “n” number, or number of monomer repeats.

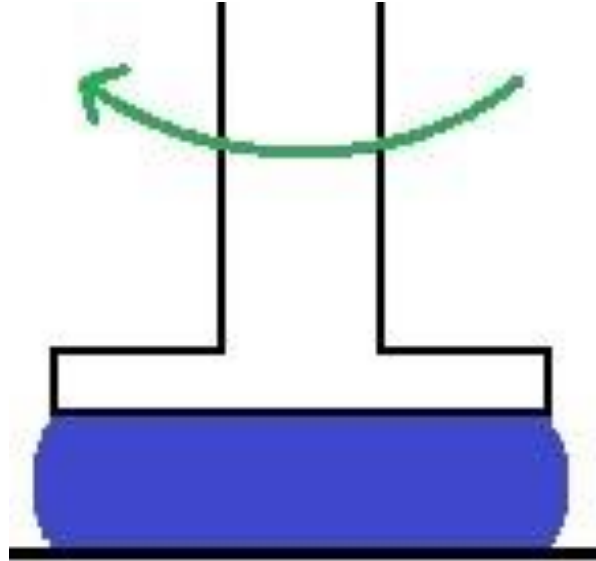


Figure 2: Basic diagram of Rheometry Process. The green arrow represents the direction of motion and the blue represents the sample. Rheometry works by pressing down against a sample and twisting at different frequencies. The rheometer measures the angular displacement, the rate of angular displacement, and the torque. Knowing those variables, the complex modulus can be calculated.

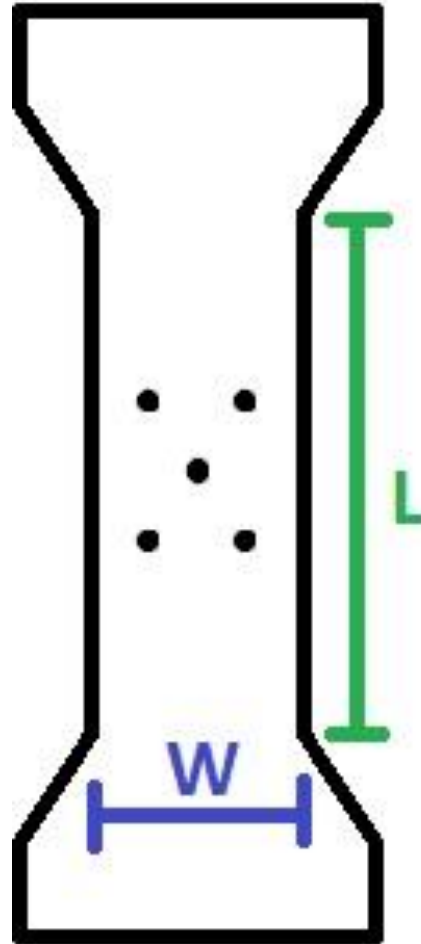


Figure 3: Diagram of Dog Bone Sample with Approximate Dimensions. Each sample was cut by hand, so some variation existed. Samples measured an average of 13 mm wide (W), 2.75 mm thick, and 45 mm long (L). The 5 dots on the sample were painted on with black nail polish and used for the non-contact strain measurement system.

### Polymer Attachment Assay

Rheometry samples that were not selected for material testing were cleaned in 95% ethanol and dried with nitrogen gas. Samples were exposed to ultraviolet (UV) light for 10 minutes. Upon completion of UV treatment, PDMS disks were incubated with 100  $\mu$ L of 10 ng/ $\mu$ L Fn for an hour before being rinsed in deionized water and moved into a 6 well plate with 2 mL cell culture medium. 40,000 cells were seeded onto the surface and cells were cultured for 24 hours. Finally, the samples were fixed and stained using the fixing protocol and immunofluorescence staining techniques described below.

### Fabricating Post Negative Molds

Microfabricated posts are made by casting a silicon wafer positive mold as previously described [23]–[26]. To summarize, the pattern of posts was first etched onto a chrome-coated quartz mask with a microPatternGenerator 101 from Heidelberg Instruments. After spin-coating a silicon wafer with Su-8 5, the mask and wafer were aligned and exposed to UV light with a MA65 mask aligner from Karl Suss. Next the wafer was cleaned with isopropyl alcohol and hard baked at 200 °C for 30 minutes. This resulting positive master mold was then used to create negative molds. 50 g of Sylgard 184 was mixed at a 10:1 polymer-to-cross linker ratio for at least 5 minutes and desiccated until no air bubbles remain. The positive mold was placed in a small aluminum tin and the desiccated PDMS was poured on top of the wafer, completely covering the wafer. After desiccating one more time to remove all air bubbles, the molds were placed in the oven for 10 minutes. After partially hardening, the positive mold was cut out of the PDMS, then stored carefully while the PDMS negative mold was placed back in the oven for 24 hours. After

24 hours, the molds were cut down to size (0.5-1 cm<sup>2</sup>) and treated with (tridecafluoro-1,1,2,2-tetrahydrooctyl)-1-trichlorosilane twice in order to non-stick the molds [23], [24].

### Fabricating Posts from Negative Molds

One of three PDMS blends were used to fabricate posts: the 10:1 184 PDMS, the 3:1 184:527 blend, or the 1:1 184:527 blend. Each of the ratios were used to create posts 5 $\mu$ m tall (#5 posts) while only the 10:1 PDMS and 3:1 blends were selected to fabricate 7 $\mu$ m tall posts (#7 posts). To generate the posts, a glass coverslip (25mm diameter) was UV treated for 5 minutes. After UV treatment, one drop of PDMS was placed on each glass coverslip and a negative mold was placed onto the drop of PDMS. The PDMS was allowed 24 hours to cure at 110°C. After curing, the negative molds were cut and lifted from the glass slides and stored in a petri dish at room temperature until use.

### Finite Element Analysis Model of Microfabricated Post Arrays

A small section of posts was modeled in Autodesk Inventor to computationally confirm the stiffness of posts. Dimensions and the elastic modulus of the posts had to be scaled up due to the constraints with Autodesk Inventor. A square was made and extruded (25mm x 25mm x 1mm) and a field of posts 2.2 mm in diameter were then made in a 9 x 9 grid on top of the 1mm thick extruded square. Posts were 5.2mm from center to center and either 5 mm (Figure 5a) or 7 mm tall. To compensate for this increase of size, the PDMS moduli were decreased by a factor of 10<sup>6</sup>. After generating the model, a force of 1N was applied to the top of one of the posts while the bottom of the base was constrained. Displacements were generated from the strain analysis software built into Autodesk Inventor (see Figure 5b for force and constraint setup).

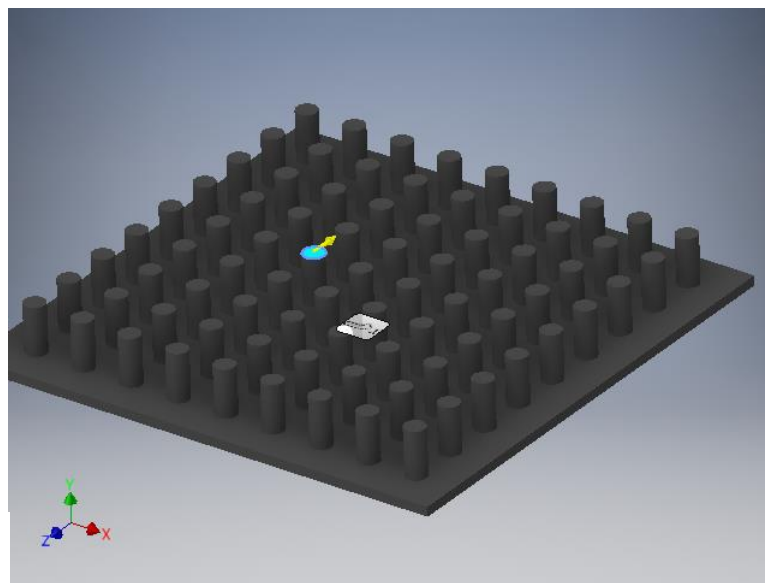
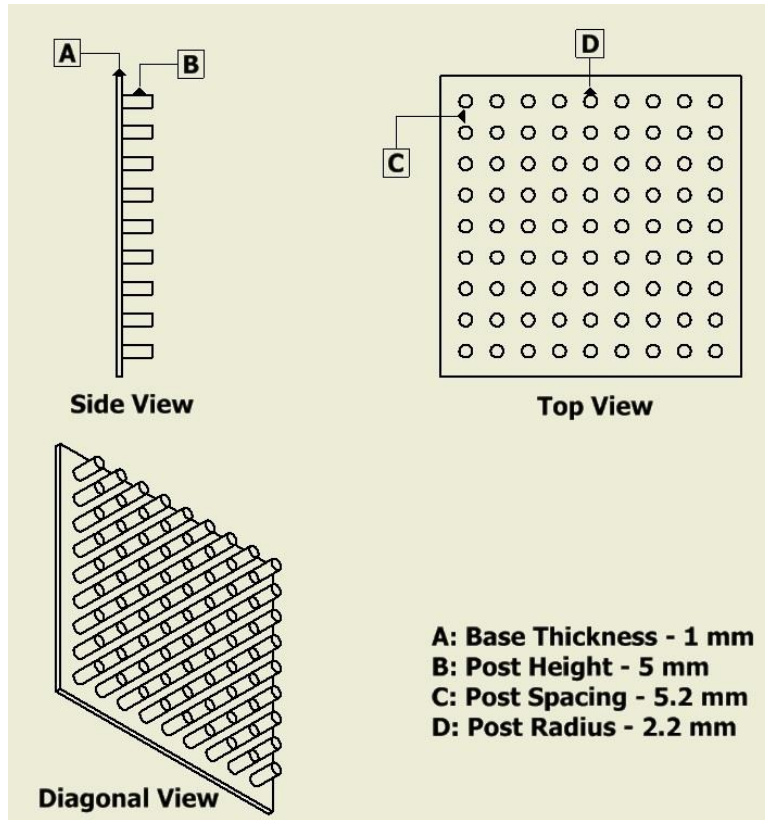




Figure 4: 3D Model of PDMS Posts. A) Schematic of the post model. All dimensions were increased due to limitations of Autodesk Inventor ( $1 \text{ mm} = 1 \mu\text{m}$ ). B) Force and Constraint Setup. The Force acted on the bright blue surface in the direction of the yellow arrow with a magnitude of 1 N. The model was constrained at the bottom of the 1 mm extruded square.

Everything aside from that face of the model was free to move in any direction.

### Preparing the Posts for Cells

To use the posts, first a square stamp of 30:1 base-to-cross-linker 184 PDMS large enough to cover the field of posts was cut from a large Petri dish and cleaned in 70% ethanol. After drying with nitrogen gas, 100  $\mu$ L of 200 nM Fn was pipetted onto the squares and allowed to non-covalently adsorb to the stamp for an hour. Subsequently, the posts were UV treated for 5 minutes. Stamps were rinsed in deionized water and dried again with nitrogen gas. Stamps were brought into conformal contact (with Fn side down) with the posts. The stamps were removed and discarded while the posts were placed into a 95% ethanol wash, a 70% ethanol wash, then three 1x PBS washes for between 5 and 30 seconds each (see Figure 6). Upon completion of the washes, posts were placed in fluorescently-tagged BSA for an hour. Three more rinses of 1x PBS followed by an hour incubation in 2% F127 Pluronics followed the BSA-488 incubation. Finally, three more rinses in 1x PBS preceded a 1x PBS bath until cells were ready to be seeded. Once the cells were lifted and counted, 40,000 cells were seeded onto each set of posts used in the experiment.

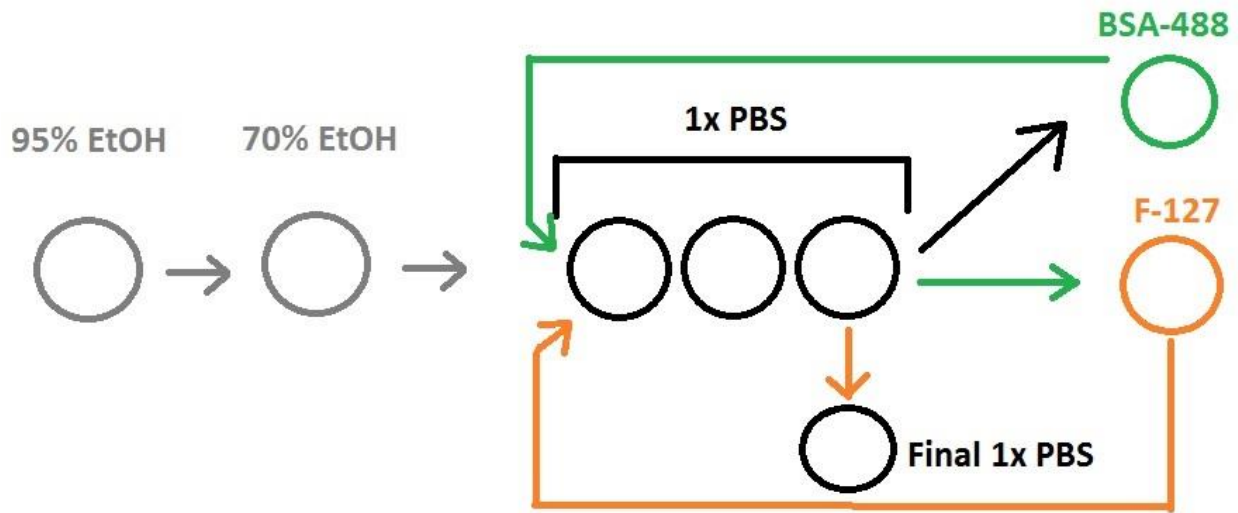


Figure 5: Post Rinse Diagram. First in gray, ethanol washes are used to both clean the posts and gradually step up the surface tension so the posts will not collapse when they are exposed to the 1x PBS. Next in black, the posts are rinsed three times in the 1x PBS. After leaving (black arrow) the posts are treated with BSA-488. The green arrow then shows the posts going through the three 1x PBS washes again, followed by the F-127 wash. Finally, the orange arrow shows the posts going through the three 1x PBS washes for a final time then being placed in a new 1x PBS wash until ready to be used.

### Fixing Samples

Paraformaldehyde was used to fix samples. Samples were taken out of the experimental environment and rinsed twice in 1x PBS. Following the rinses, samples were placed in a triton/paraformaldehyde solution (0.5 mL 10% Triton-X100 mixed with 9.5 mL 4% Paraformaldehyde) for 2 minutes then were placed in 4% paraformaldehyde for 20 minutes. Two more rinses in 1x PBS were completed, then samples were placed into 1x PBS until they were ready to be stained.

### Immunofluorescence Imaging

Preparations for staining started by placing the fixed samples in 0.1% BSA for 5 minutes. During this time, a staining chamber was created by placing filter paper on the bottom of a petri dish with an area of 100 cm<sup>2</sup>. After deionized water was used to moisten the filter paper, a layer of parafilm was used as the top layer of the staining chamber. Primary and secondary antibody solutions were made to stain actin and fibronectin. In the primary antibody solution, 1.25 µL of rhodamine phalloidin 555 and 0.5 µL rabbit-α-Fn primary antibody were added to 48.25 µL of 0.1% BSA (per sample). 2 µL of AF647-α-rabbit added to 48 µL of 0.1% BSA (per sample) was mixed to create the secondary antibody solution. To immunofluorescently stain the samples, 50 µL of the primary antibody solution were pipetted onto the parafilm of the staining chamber and the samples were placed cell side down onto the drops. The staining chamber was placed into a 37 °C oven for 30 minutes. Samples were removed after 30 minutes and placed cell side up into 0.1% BSA for 5 minutes again and the staining chamber was cleaned. This process was repeated for the secondary antibody solution. After placing the samples into 0.1% BSA again, 2 drops of DAPI nuclear stain per mL BSA were placed into each sample and allowed to sit for 5 minutes.

### Mounting Samples

Glass coverslips (25 mm in diameter for polymer attachment assays and 12.5 mm in diameter for posts) were rinsed in 70% ethanol and dried. 5  $\mu$ L of fluoromount (floromount-g for posts) were pipetted onto each coverslip and the samples were placed cell side down onto the fluoromount. Samples were incubated for 1 hour at room temperature in the dark. Samples were either imaged or wrapped in aluminum foil and placed into the 4 °C refrigerator until it was time to image the samples.

### Matlab Analysis

Code written previously was used to gather data from polymer attachment assays and post force experiments. Images taken from each sample were converted into grayscale high quality tagged image file format (.tif). These .tif images were then examined by image processing software in built into Matlab to find boundaries of cells, Fn fibrils, and number of nuclei in the case of polymer viability assays. For post experiments images of the tops and bottoms of the posts were processed and the centroids were found. Using the displacement of the centroids and equation 3, cellular forces were found. Matlab uses Equation 3 to calculate the force on each post. Calculating cellular forces is done by first making a mask of where the cells are located using actin staining, then using that mask to select only posts that are located underneath cells. Posts under the direct influence of cells are then marked by the Matlab code and their centroids are found. Changes in the position of the centroids are measured as displacement due to a cell's influence and converted into a force vector, which is then reported.

### Culturing Cells

Cells used in all experiments were normal human lung fibroblasts (NHLFs) and were cultured using the FGM<sup>TM</sup>-2 BulletKit<sup>TM</sup>. Media was changed every 24 hours and cells were cultured at 37 °C and 5% CO<sub>2</sub> concentration.

### Statistical Testing

To determine statistical significance, one way ANOVA tests were performed for polymer attachment assays as well as post force data. T-Tests to compare each of the sets of data. P-values less than 0.05 were considered to be significant.

### Chapter 3: Results

Complex shear moduli for Pure PDMS polymers are displayed in Figure 6A, with Figure 6B showing the PDMS Blend complex shear moduli. Data was collected from 6 independent samples. Results show that the modulus of Pure PDMS polymers decreases as a function of 184 cross-linker density (Figure 7A). Complex shear modulus values of the PDMS Blend polymers increase as the percent of Sylgard 184 increases in the polymer (Figure 7B). These two points help show that the stiffness of Sylgard 184 Pure PDMS polymers can be “cut”, allowing for polymers that are stiff enough to use in post fabrication but soft enough to lower the effective modulus of the posts. Figure 8 shows the complex shear modulus values of each of the polymers used in post fabrication.

Tensile testing was performed to gather Poisson’s ratio and verify rheometry data. Samples were clamped into a Bose ElectroForce<sup>®</sup> 3230 and testing rate was set to 10 mm/min. As the test ran, the longitudinal strain, lateral strain, and force data was measured and recorded. To find the elastic modulus of our samples, the force data was divided by the cross-sectional area of each sample, then the slope of the stress-strain curve was found using Microsoft Excel. The slope of the stress-strain curve in the linear, elastic region of a polymer is the elastic modulus for that sample. Poisson’s ratio was also found by taking the slope of the longitudinal strain vs the lateral strain. Figure 9A shows the results of tensile testing, and 9B shows tensile testing elastic modulus values compared to rheometry elastic modulus values. Rheometry elastic modulus values were found by using equation 5, where  $E$  is the elastic modulus,  $G$  is the complex shear modulus, and  $\gamma$  is Poisson’s ratio. To account for curing temperature differences, elastic modulus values were normalized to 10:1 Pure PDMS. Normalized values shown in Figure 9C and Figure 9D shows differences between the normalized elastic modulus values.

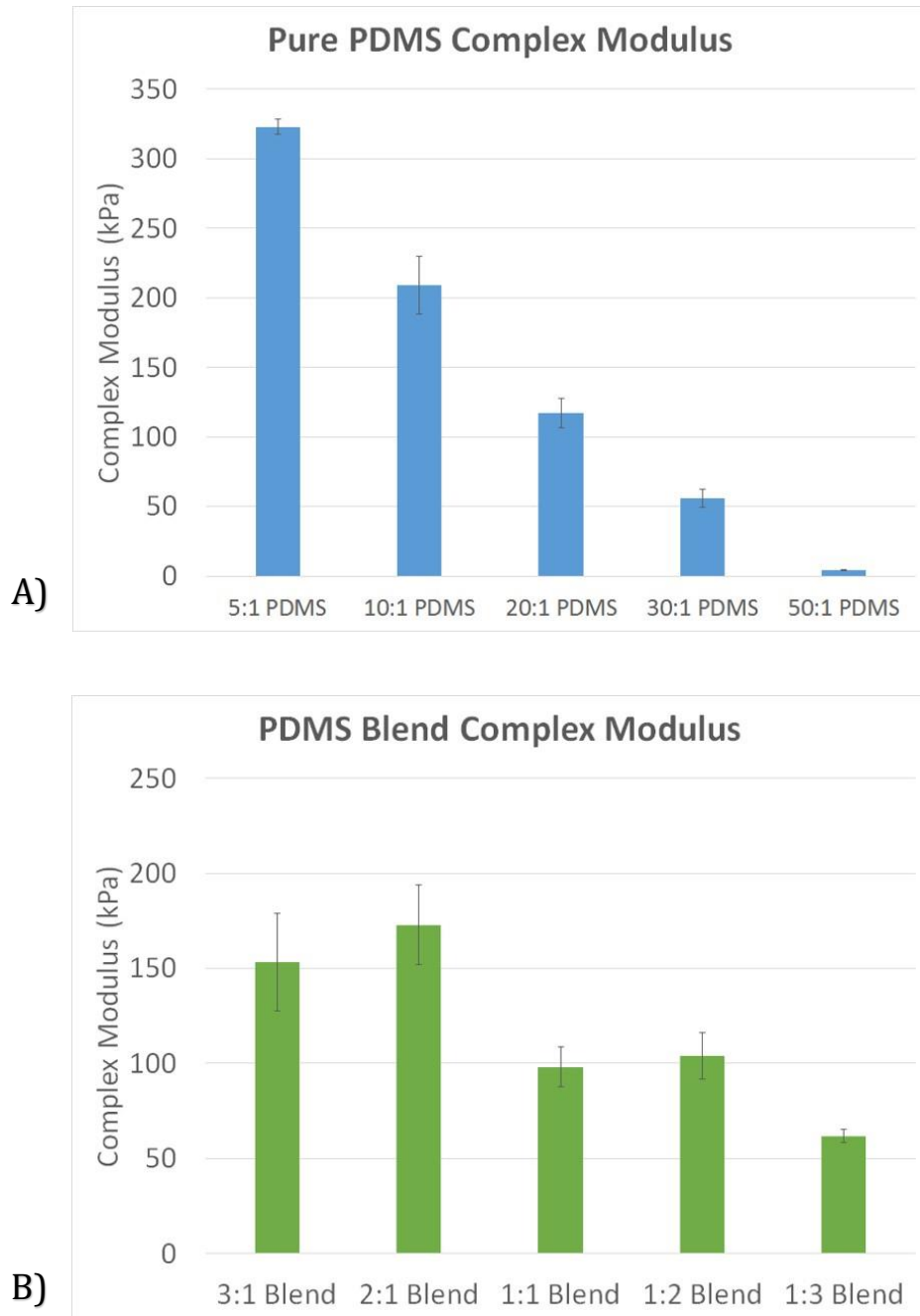


Figure 6: Complex Shear Modulus Values for All Pure PDMS and PDMS Blends. A) Complex shear modulus values for all Pure PDMS polymers. Pure PDMS contains only Sylgard 184 base and cross-linker. B) Complex shear modulus of PDMS Blends. PDMS Blends contain both Sylgard 184 (10:1) and Sylgard 527 (1:1)



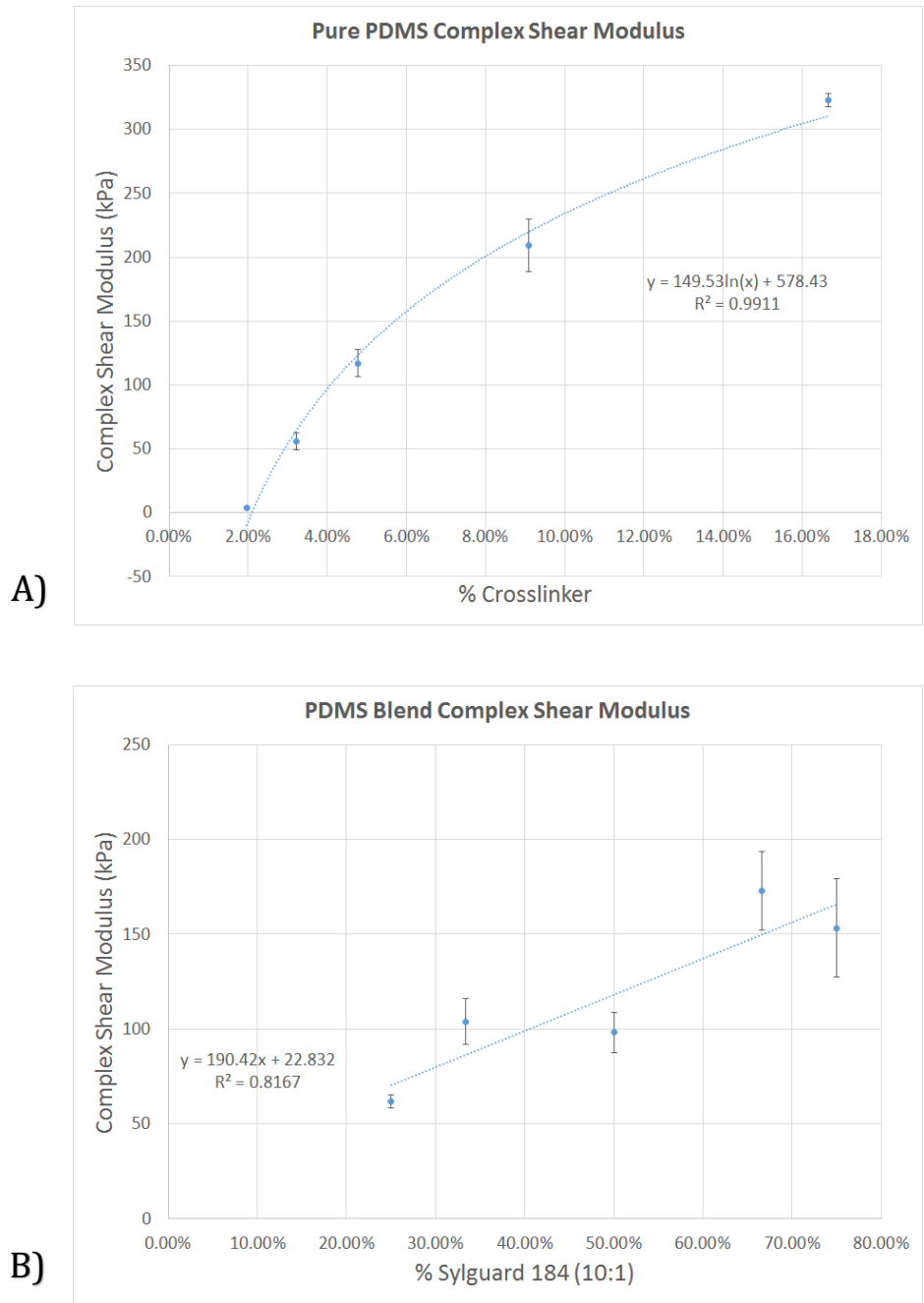


Figure 7: Complex Shear Modulus Values as a Function of Polymer Percent Composition. (A) Pure PDMS complex modulus as a function of percent cross-linker. A value of 9% is equivalent to 10:1 Pure PDMS polymer. (B) PDMS Blend complex shear modulus as a function of percent Sylgard 184. A value of 75% Sylgard 184 is equivalent to the 3:1 PDMS Blend. N=6

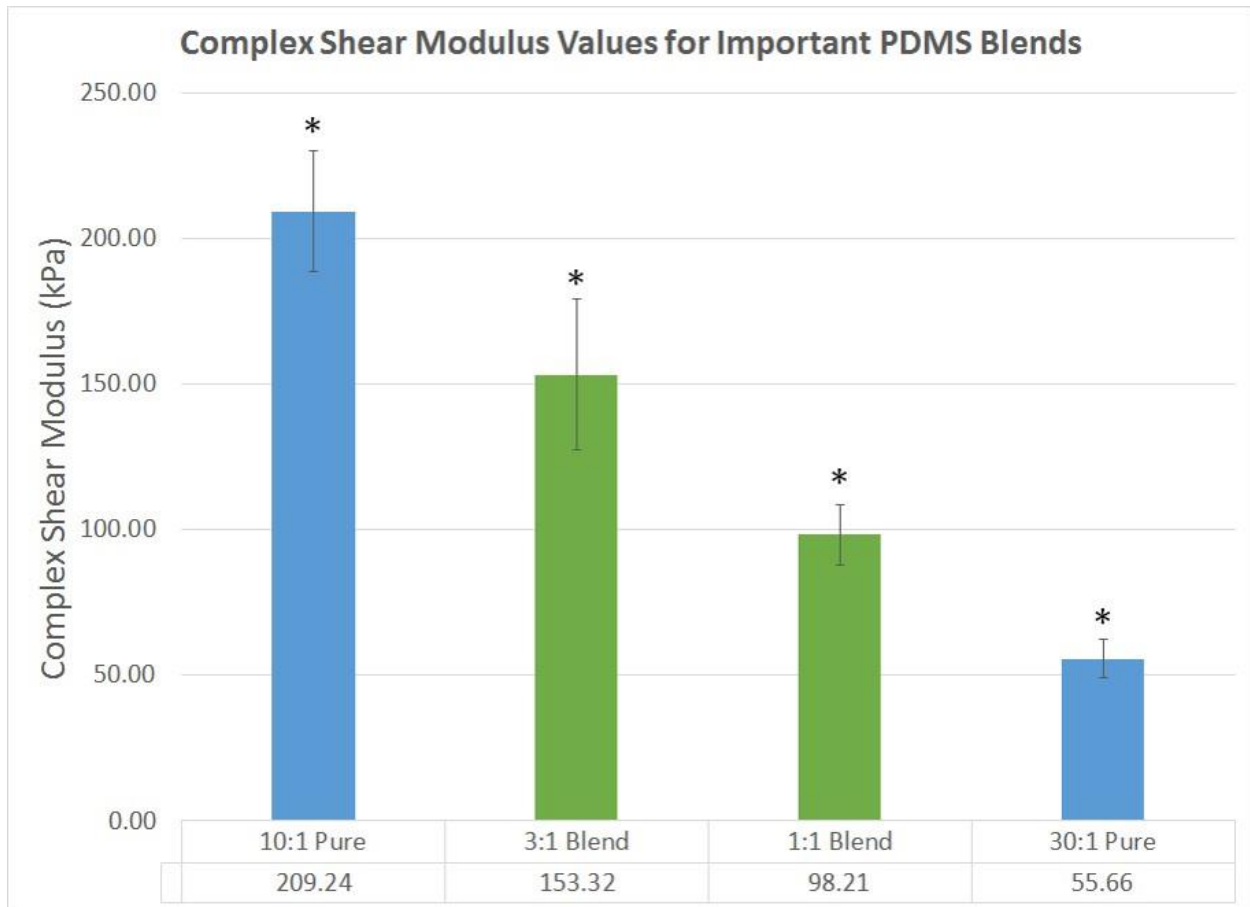
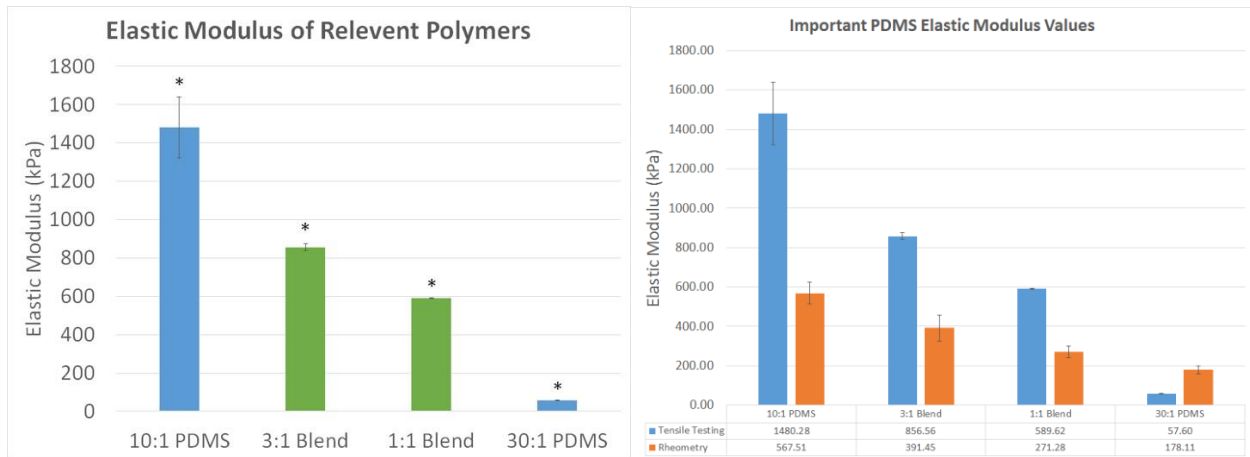
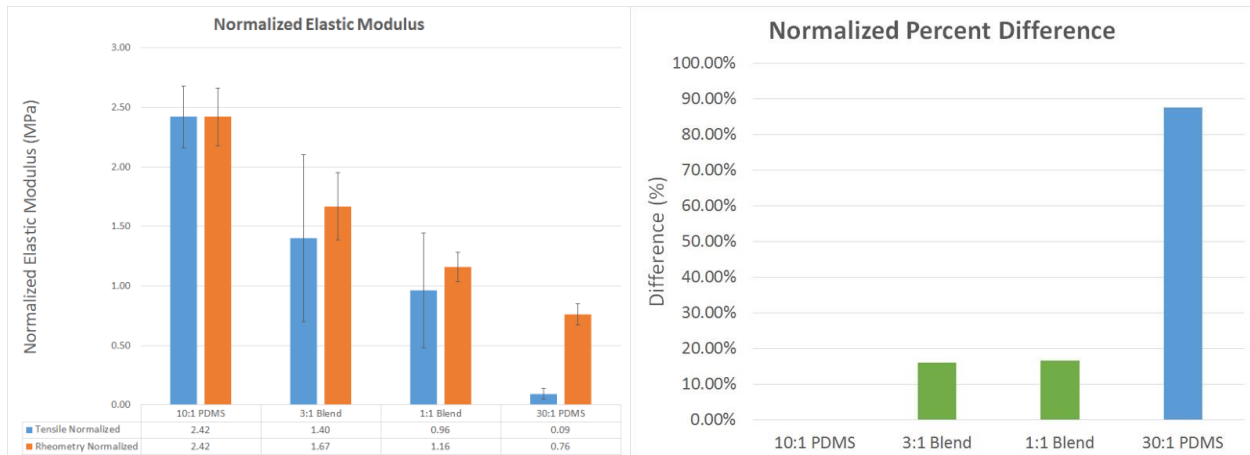


Figure 8: Important PDMS Complex Shear Modulus Values. The values displayed in this figure show only Pure PDMS (blue) and PDMS Blends (green) involved in fabrication of posts or stamps. N=6 \*p<0.05 There was a statistically significant effect of PDMS Blend ratio on stiffness (one-way ANOVA, p<0.05)



A)

B)



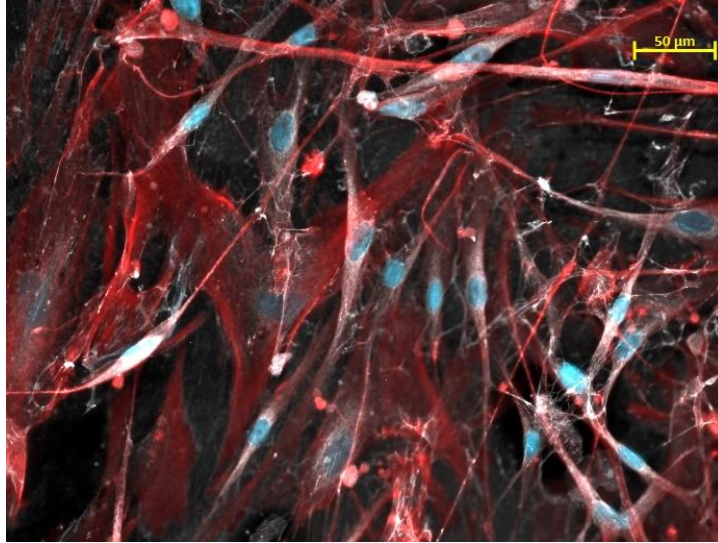
C)

D)

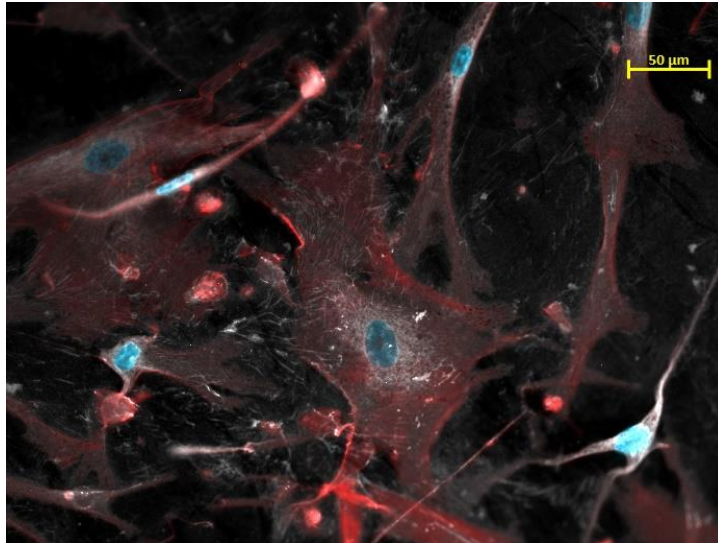
Figure 9: Elastic Modulus Data of PDMS Polymers Used in Micropost Fabrication. A) Elastic modulus values from tensile testing in units of kPa. Blue bars are Pure PDMS and green bars are PDMS Blends. B) Comparison of tensile testing results (blue) and rheometry results (orange). C) Normalized elastic modulus of both rheometry and tensile testing results. D) Percent difference between normalized tensile testing and rheometry elastic moduli. N=6. \* $p < 0.05$  There was a statistically significant effect of PDMS Blend ratio on stiffness (one-way ANOVA,  $p < 0.05$ )

After all mechanical data was collected, polymer attachment experiments were conducted to determine cell performance on both the Pure PDMS and the PDMS Blend polymers. Images of actin, nuclei, and Fn were collected; representative images are shown in Figure 10. An original image processing algorithm written in Matlab was used to determine nuclear count, measure the average cell area, and measure the area of Fn fibril area relative to the total area of the image (Figure 11). The number of nuclei present was lower in the blends of PDMS when compared to the normal ratios of PDMS and the cell area was much smaller. Another property measured was the assembled Fn. The area percent of the Fn was about the same as the softer PDMS Blends and Pure PDMS polymers, however showed a large increase when compared to the 10:1 ratio. Having both characterized the mechanical properties of the PDMS blends, and determined that cells were able to attach to and assemble Fn onto each Pure PDMS and PDMS Blend, we next moved on to determining the mechanical properties of posts using 3D modeling. Stiffness values of posts were attained from Autodesk Inventor modeling using built in finite element analysis software. An example of the force and constraint setup for the model is shown in Figure 12 along with a table of stiffness values found. These values were used in Matlab to calculate cellular forces. Using these new stiffness values in a Matlab model, cellular force data could be calculated from acquired post experiment images. Examples of images from post experiments can be found in Figure 14 and 15. Figure 13 shows a sketch of the post deflection imaging strategy.

A)



B)



C)

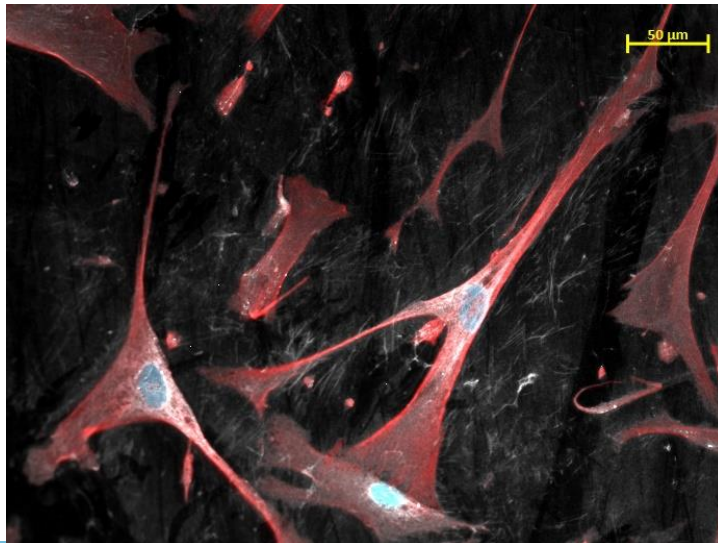


Figure 10: Representative immunofluorescence images for (A) 10:1 Pure PDMS, (B) 3:1 PDMS Blend, and (C) 1:1 PDMS Blend. Images show a composite of red (actin), blue (nuclei), and white (Fn). Scale bar = 50  $\mu$ m.

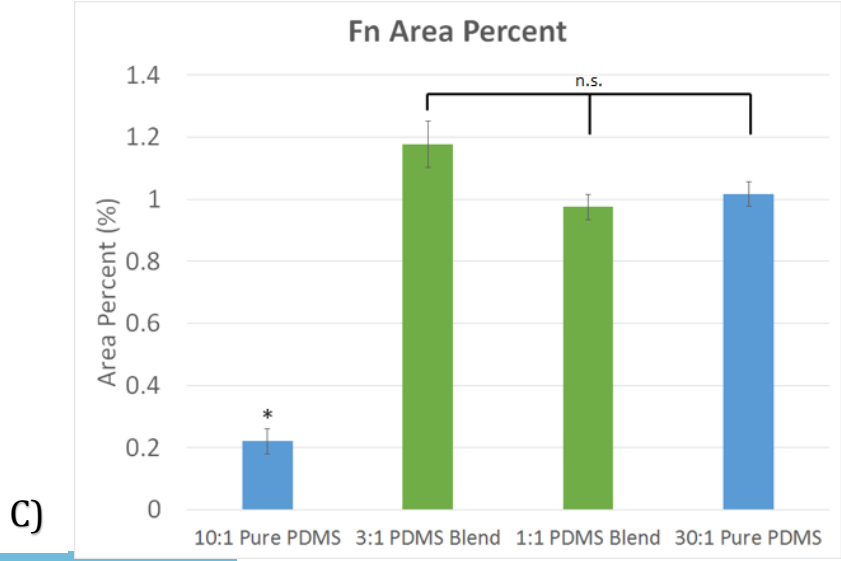
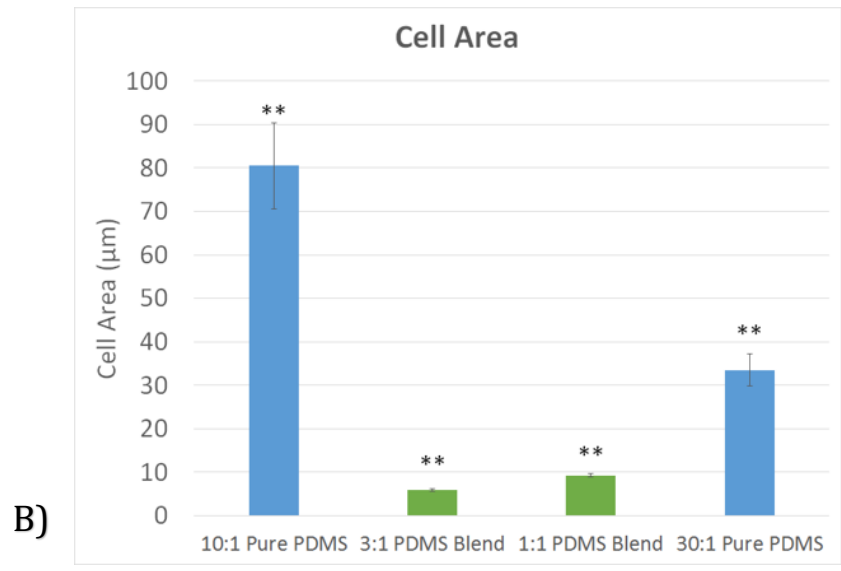
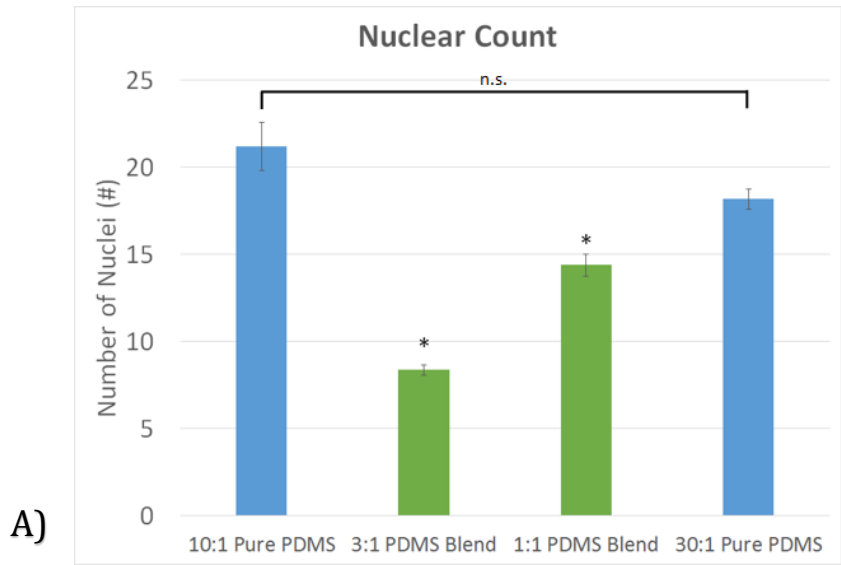
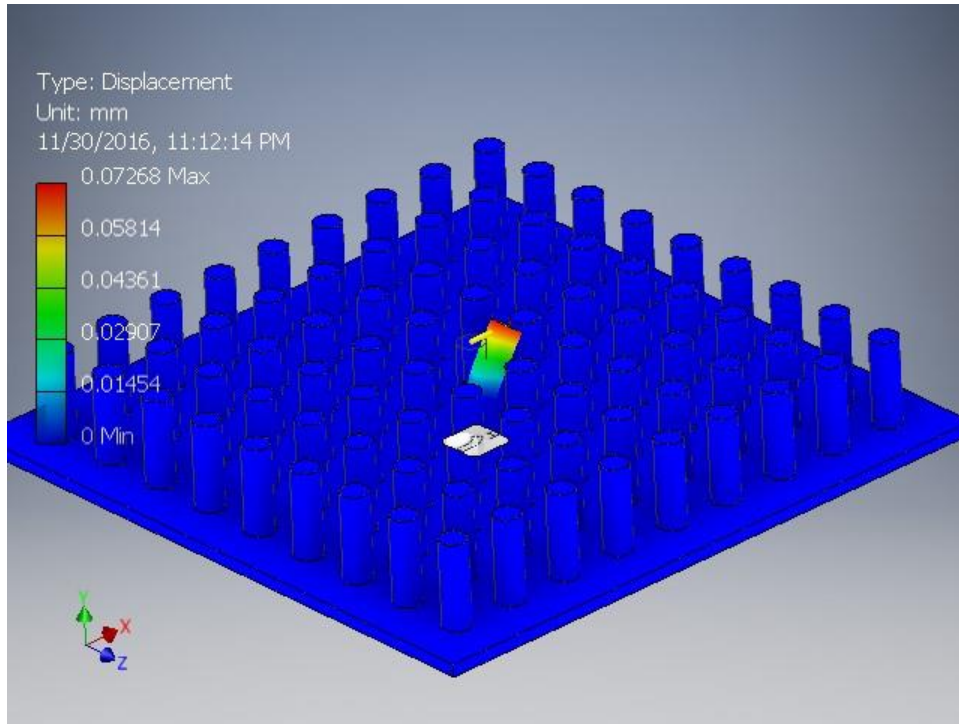


Figure 11: Polymer Attachment Assay Results. (A) Average number of cells per microscope field for each of the PDMS blends. (B) Cell area. (C) Fn area percent.  $N > 16$ . \* $p < 0.05$ , \*\* $p < 0.005$  There was a statistically significant effect of PDMS type on cell area, Fn assembly, and Nuclear count (one-way ANOVA,  $p < 0.05$ )





	Estimated Stiffness (nN/ $\mu\text{m}$ )	Modeled Stiffness (nN/ $\mu\text{m}$ )	Percent Difference (%)
<b>#5 - 10:1 Pure PDMS</b>	46.92	49.19	4.84
<b>#5 - 3:1 PDMS Blend</b>	32.36	33.23	2.70
<b>#5 - 1:1 PDMS Blend</b>	22.43	23.66	5.50
<b>#7 - 10:1 Pure PDMS</b>	17.10	18.44	7.88
<b>#7 - 3:1 PDMS Blend</b>	11.79	13.76	16.66

Figure 12: Autodesk Inventor Strain Model. Inventor results from the strain simulation are shown graphically and in the table above. Graphic display is from the #7 – 3:1 PDMS Blend simulation

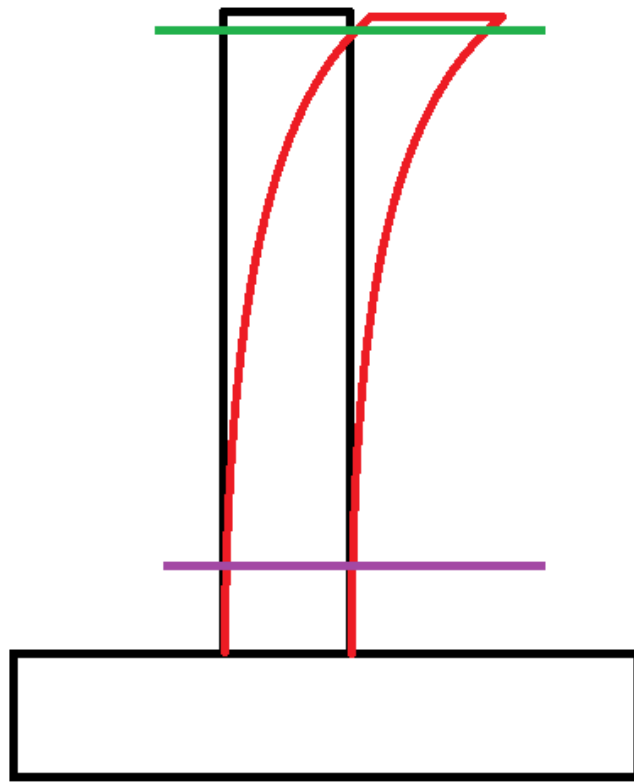
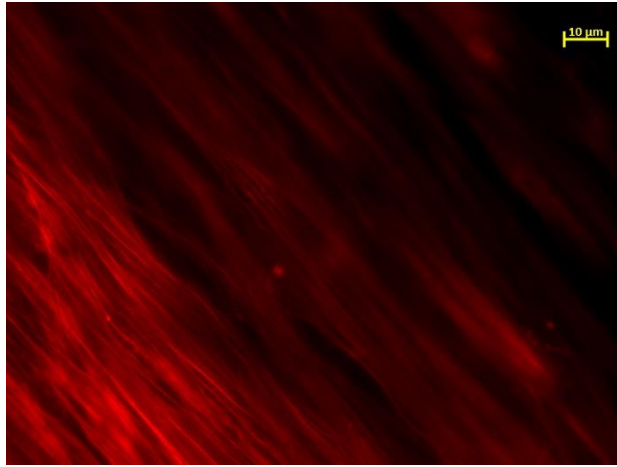
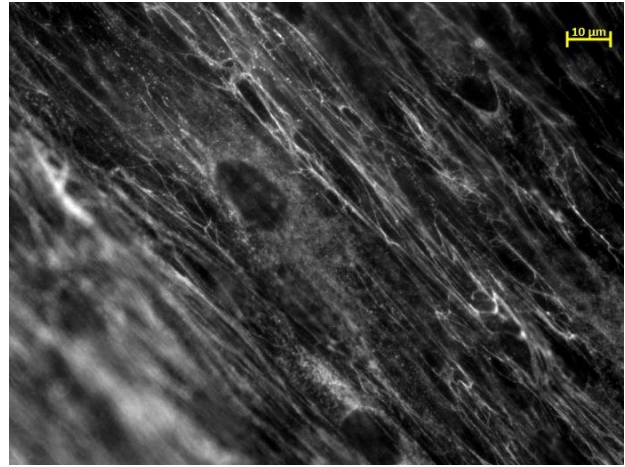


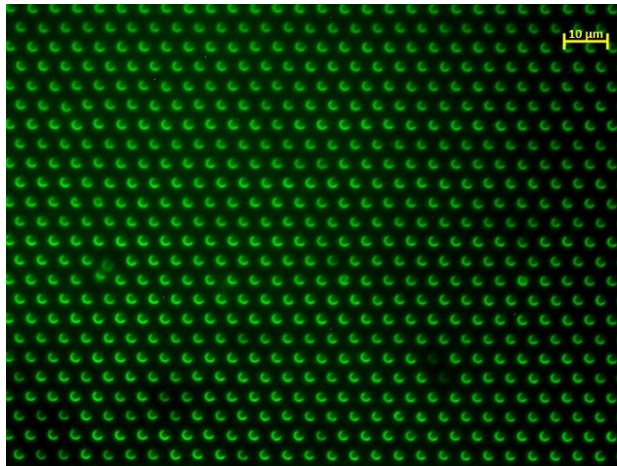
Figure 13: Post Imaging Strategy Example. The green line shows approximately where the top image of posts is taken. The line has been lowered slightly to make it easier to see the tops of the post in the drawing. The purple line shows where the bottom post image is taken.



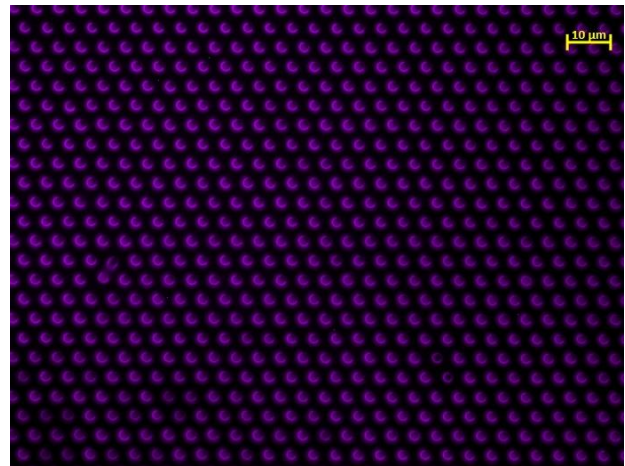
A)



B)



C)



D)

Figure 14: #7 Posts, 3:1 PDMS Blend. (A) Actin (B) Fn (C) Post tops (D) Post Bottoms

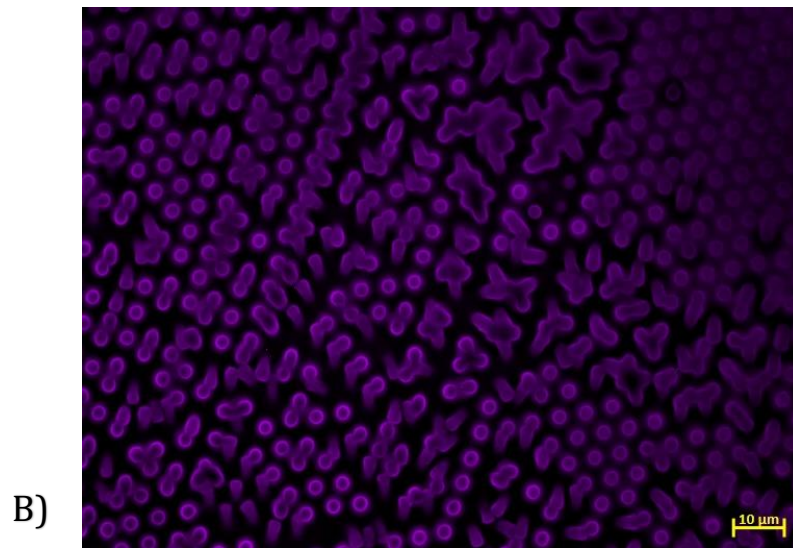
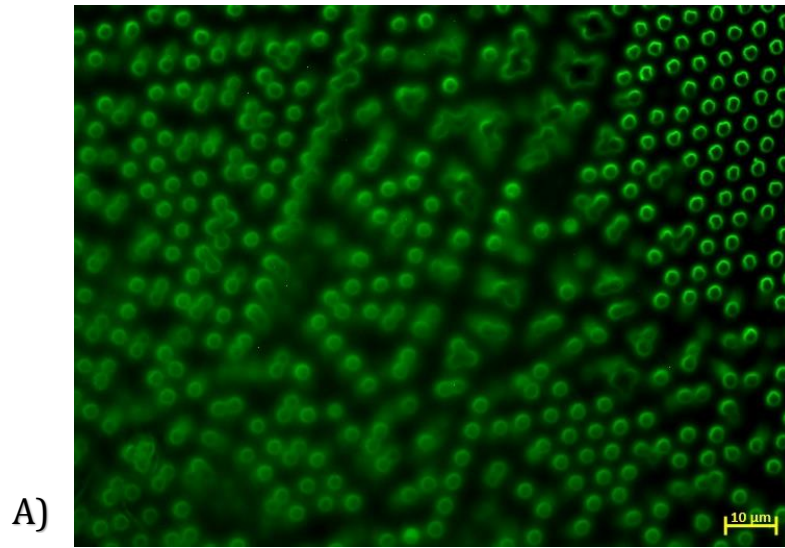
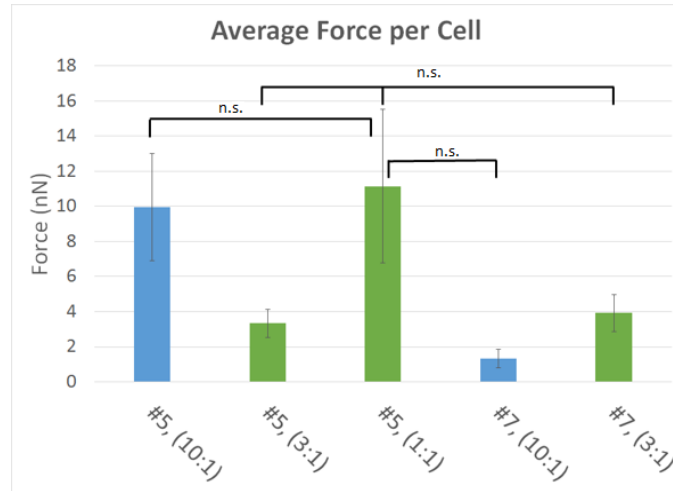


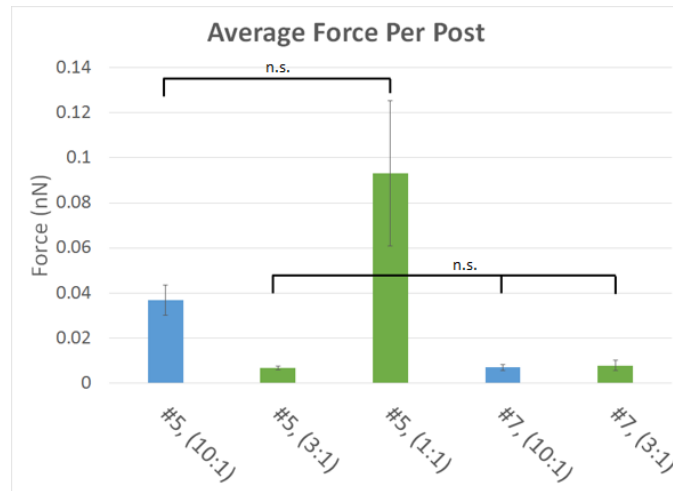
Figure 15: #5 Posts, 1:1 PDMS Blend. (A) Post Tops (B) Post Bottoms

After images were collected, an original force analysis algorithm written in Matlab was used to find the magnitude of force that a cell exerts onto the substrate. Shown in Figure 16A, it was found that the average force per cell tended to decrease as the post stiffness decreased. Force per post data in Figure 16B agrees except for the #5, 1:1 PDMS Blend posts. An example of the posts can be seen above in Figure 14.

A)



B)



C)

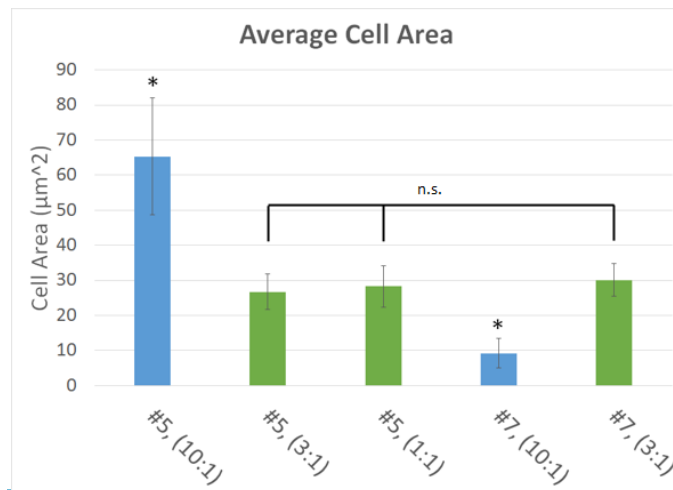


Figure 16: Force Data from Post Experiment. (A) Average force per cell. (B) Average force per post. Except for #5, 1:1 PDMS Blend, the softer substrates had lower forces per post than the #5, 10:1 Pure PDMS sample. (C) Average Cell Area. N= #5, 10:1 Pure PDMS – **7**; #5, 3:1 PDMS Blend – **16**; #5, 1:1 PDMS Blend – **5**; #7, 10:1 Pure PDMS – **27**; #7, 3:1 PDMS Blend – **18** \* $p < 0.05$ . Groups that had no statistically significant difference are marked. Statistical differences with  $p < 0.05$  were found between different groups. There was a statistically significant effect of post type on cell area, force per post, and force per cell (one-way ANOVA,  $p < 0.05$ )

## Chapter 4: Discussion

Blends of Sylgard 184 and Sylgard 527 should generate biomaterials with mechanical properties that appropriately simulate physiological stiffness. To characterize these blends, we conducted mechanical testing aimed at quantifying mechanical properties. Traditionally, the way Pure PDMS was softened was by changing the ratio of base polymer to cross-linker. We wanted to avoid doing this due to cytotoxic effects of excess polymer base or cross-linker. Making posts from softer Pure PDMS would not only have potentially cytotoxic effects [27], but any Pure PDMS would be far too soft to make posts out of. Negative molds would be destroyed and large areas of posts would be collapsed before they would be used. Subjectively, it was found that PDMS Blends tended to be much more “brittle” and would flake apart much more readily than the Pure PDMS polymers, even at the 1:3 PDMS Blend. This could be due to the molecular makeup of each type of PDMS. When making a Pure PDMS polymer, the units making up the bulk material are all uniform. By introducing polymer chains of two different lengths, imperfections form in the material which could cause it to be more brittle. Tensile testing also showed that all the PDMS Blends failed abruptly while the Pure PDMS samples did not fail during testing.

Complex moduli of Pure and Blend polymers were collected via rheometry using a DHR Rheometer from TA Instruments set up for a small amplitude oscillatory shear test. As the upper plate of the rheometer applied a sinusoidal strain over the range of 1 to 100 rad/sec, the sinusoidal stress was measured and resolved into components in phase and  $\frac{\pi}{2}$  out of phase with respect to the input. Stress in phase with the input was recorded as the shear elastic response ( $G_E$ ), while the out of phase stress was recorded as the shear viscous response ( $G_V$ ). The complex shear modulus ( $G$ ) could then be calculated from the two outputs of the rheometer by using the



equation 4 [28]. The complex shear modulus at the lower frequency (1 Hz) was used as the most relevant frequency. All calculations converting shear modulus to elastic modulus used this lower frequency complex modulus.

Values recorded from all material testing were lower than values recorded in literature. Lower temperature during the curing process also cause the elastic modulus of PDMS to decrease [29]. Rheometry seemed to produce lower elastic modulus values than tensile testing. This could be because the complex modulus is a combination of the storage and loss moduli of a material undergoing oscillating loads. During repeated loading, the material may become fatigued and material properties may change causing slightly lower modulus values. Tensile tests did not cycle loading in this experimental setup, so material fatigue was avoided. More testing using PDMS cured at higher temperatures will shed light on this discrepancy. To account for the difference between elastic modulus values, each polymer's elastic modulus was normalized with respect to the Pure PDMS (10:1) polymer. It is important to point out that all the PDMS Blend samples failed during tensile testing. The point of failure was close to the clamps, suggesting that there may have been an uneven stress distribution across the sample. Even though this could cause some variability in the modulus values, it suggests that there may be more brittle properties of Blends when compared to Pure PDMS. Further testing to characterize these properties are required before any conclusions can be made.

During polymer attachment assays some differences between cell size, Fn assembly, and nuclear count were observed. Even with some differences between cell numbers and size, it was concluded that cells were able to attach to and assemble Fn on both Pure PDMS or PDMS Blends. Differences between cell area and numbers could be due to the change of substrate stiffness. Though the PDMS Blends did not seem to affect the ability of cellular attachment; size

and number of cells on the Blends did seem to change. Further studies observing expression of  $\alpha$ -smooth muscle actin, as well as cell viability experiments could help to gain an understanding on differences between cells on PDMS Blends and Pure PDMS.

Post calibration was used to get the most accurate stiffness values to use in our Matlab model. To get accurate stiffness values, multiple posts had to be modeled on top of a small layer of PDMS as a base. This is because the posts are continuous with a small layer of PDMS on top of glass slides. The PDMS layer on the bottom is much softer than the glass and could deform. Modeling the posts not only gave an effective stiffness for each post, but also confirmed that forces acting on the tops of posts only deform the posts, not the PDMS substrate underneath. Even though there was no deformation of the PDMS under the posts, the small discrepancies between calculated and modeled stiffness values is most likely due to the effects of this layer. Exact measurements were shown in Figure 4A and were used in each model. Values needed to be scaled for Autodesk Inventor to model the posts. Distances were increased by 1000, and to accommodate the elastic modulus of the PDMS was decreased by a factor of  $10^6$ . This factor was found by using the units of force and distance from the model (N/mm) and converting them to units found experimentally in the posts from previous studies (nN/ $\mu\text{m}$ ) [24]. A shear force with a magnitude of 1 N was applied in each experiment.

Interestingly, 3:1 PDMS Blends seemed to generate the most repeatable, successful fields of posts. As discussed above, the PDMS Blends tended to be more brittle than the Pure PDMS. This could play a role in the ease of post fabrication. During the post generation protocol, negative molds of the posts are lifted off of freshly cured positive PDMS. Pure PDMS being much less brittle tends to stretch more and adheres to the molds. PDMS Blends being more brittle will deform less during the manufacturing process, allowing them to slide out of the

negative molds easier. Though these posts are taller, therefore softer, than the #5 posts, #7 posts made from 3:1 PDMS Blends were more successful and had fewer fields of collapsed posts.

Cellular post data shows that cell area decreased as substrate stiffness went down. This decrease did seem to be dependent on both substrate stiffness and the polymer used. PDMS Blends did not show any statistically significant differences between cell areas, though they were different from posts made from Pure PDMS. Average forces per post tended to be low, and decrease as stiffness decreased. The exception to this was #5 posts made from 1:1 PDMS Blends. This could be due to the large amount of collapsed posts on each sample skewing data. Forces per cell seemed to vary widely between samples, though cells on lower stiffness posts seemed to generate lower forces

## Chapter 5: Conclusions and Future Directions

Finding softer substrates with the ability to measure cellular forces was attempted to create new physiologically relevant models for investigating cellular forces (between 0.5 kPa and 4 kPa). Rheometry and tensile testing produced elastic moduli for PDMS Blends which were used as parameters in the post models made in Autodesk Inventor. Finite element analysis on the models from Autodesk Inventor simulation software provided the post stiffness for each new PDMS Blend proposed in this study. Finally, posts were fabricated using these new PDMS Blends and force data from NHLF cells was compiled.

Rheometry data was gathered to select PDMS Blends that would be softer than the Pure 10:1 PDMS, but stiffer than the Pure 30:1 PDMS. Pure 30:1 PDMS would theoretically be able to generate 7  $\mu\text{m}$  tall posts that had an effective modulus of 1.6 kPa, but due to the material's softness, posts cannot stay upright through the processing required for cell fixing and staining. Any fields of posts that are upright would be surrounded by collapsed posts, generating data that is difficult to analyze. To combat this, 3:1 and 1:1 PDMS 184:527 Blends were selected as polymers that would be stiff enough to fabricate viable posts, while soft enough to lower the effective stiffness to physiological levels. After selecting the PDMS Blends that would be used, tensile testing was completed to confirm the elastic modulus of the materials.

After quantifying mechanical properties, polymer attachment testing was completed to ensure cells could survive on the polymer surfaces. Interestingly, the cells survived on all surfaces even though there were some differences in cell size and count. Some of these differences could be due to the change in substrate stiffness, but more studies are required to understand exactly what is changing between the Pure PDMS and the PDMS Blends. Though changes in cellular morphology and density were observed, cells were able to attach to the

PDMS surface and survive. Posts were made using each of the blends and cells were seeded successfully. Imaging the posts showed that cells could attach successfully to each post type tested. Reduced cellular contact with posts helps to reduce the effects seen from the polymer attachment experiments.

Results from this study show that PDMS blends could be a viable replacement for 10:1 Pure PDMS in any micropillar array assays. By using the new PDMS Blends, posts would be more physiologically relevant and easier to fabricate. This could be a useful tool in gaining insights into the mechanical properties of fibrosis. Understanding and perfecting the methods of controlling substrate stiffness and measuring cellular forces allow another dimension of characterization of disease states. For example, comparing the forces generated by healthy fibroblasts versus those from patients with fibrotic disease could shed light on new angles of treatment, while comparing NHLF cells that are healthy to COPD disease state NHLF cells could help shed light on the loss of functionality of lung tissue and open a potential treatment avenue. Cellular forces, extracellular matrix assembly, and substrate stiffness are all imperative for normal tissue function. When regulation of these systems fail, the resulting fibrosis can reduce cell, tissue, and organ function to the point of patient mortality. Healthy and disease state substrates act very differently, so being able to fabricate a tool to measure cellular forces while remaining faithful to physiological stiffness could have far reaching implications in many fields of medicine.

## References

- [1] T. A. Wynn, “Fibrotic disease and the TH1/TH2 paradigm,” *Nat. Rev. Immunol.*, vol. 4, no. 8, pp. 583–594, Aug. 2004.
- [2] B. Rybinski, J. Franco-Barraza, and E. Cukierman, “The wound healing, chronic fibrosis, and cancer progression triad,” *Physiol. Genomics*, vol. 46, no. 7, pp. 223–244, Apr. 2014.
- [3] T. E. King, A. Pardo, and M. Selman, “Idiopathic pulmonary fibrosis,” *Lancet*, vol. 378, no. 9807, pp. 1949–1961, Dec. 2011.
- [4] K. Raimundo, E. Chang, M. S. Broder, K. Alexander, J. Zazzali, and J. J. Swigris, “Clinical and economic burden of idiopathic pulmonary fibrosis: a retrospective cohort study,” *BMC Pulm. Med.*, vol. 16, no. 1, p. 2, Dec. 2016.
- [5] B. C. Brown, S. P. McKenna, K. Siddhi, D. A. McGrouther, and A. Bayat, “The hidden cost of skin scars: quality of life after skin scarring,” *J. Plast. Reconstr. Aesthetic Surg.*, vol. 61, no. 9, pp. 1049–1058, Sep. 2008.
- [6] C. Frantz, K. M. Stewart, and V. M. Weaver, “The extracellular matrix at a glance,” *J. Cell Sci.*, vol. 123, pp. 4195–4200, 2010.
- [7] S. K. Bhatia, *Engineering Biomaterials for Regenerative Medicine*. New York, NY: Springer New York, 2012.
- [8] A. J. Engler, S. Sen, H. L. Sweeney, and D. E. Discher, “Matrix Elasticity Directs Stem Cell Lineage Specification,” *Cell*, vol. 126, no. 4, pp. 677–689, 2006.
- [9] B. Hinz, D. Mastrangelo, C. E. Iselin, C. Chaponnier, and G. Gabbiani, “Mechanical tension controls granulation tissue contractile activity and myofibroblast differentiation,” *Am. J. Pathol.*, vol. 159, no. 3, pp. 1009–20, 2001.
- [10] B. Hinz, S. H. Phan, V. J. Thannickal, A. Galli, M.-L. Bochaton-Piallat, and G. Gabbiani,

- “The myofibroblast: one function, multiple origins.,” *Am. J. Pathol.*, vol. 170, no. 6, pp. 1807–16, Jun. 2007.
- [11] M. S. Sakar, J. Eyckmans, R. Pieters, D. Eberli, B. J. Nelson, and C. S. Chen, “Cellular forces and matrix assembly coordinate fibrous tissue repair,” *Nat. Commun.*, vol. 7, p. 11036, Mar. 2016.
- [12] M. P. Czubryt, “Common threads in cardiac fibrosis, infarct scar formation, and wound healing,” *Fibrogenesis Tissue Repair*, vol. 5, no. 1, p. 19, 2012.
- [13] W. V. Butcher DT, Alliston T, “A tense situation: forcing tumor progression,” *Nat Rev Cancer*, vol. 9, no. 2, pp. 108–122, 2009.
- [14] S. Mueller, “Liver stiffness: a novel parameter for the diagnosis of liver disease,” *Hepatic Med. Evid. Res.*, vol. 2, p. 49, May 2010.
- [15] K. E. Kubow *et al.*, “Mechanical forces regulate the interactions of fibronectin and collagen I in extracellular matrix.,” *Nat. Commun.*, vol. 6, p. 8026, 2015.
- [16] C. a. Lemmon, C. S. Chen, and L. H. Romer, “Cell traction forces direct fibronectin matrix assembly,” *Biophys. J.*, vol. 96, no. 2, pp. 729–738, 2009.
- [17] J. Y. Sim *et al.*, “Spatial distribution of cell-cell and cell-ECM adhesions regulates force balance while maintaining E-cadherin molecular tension in cell pairs,” *Mol. Biol. Cell*, vol. 26, no. 13, pp. 2456–2465, 2015.
- [18] J. L. Eisenberg *et al.*, “Substrate stiffness regulates extracellular matrix deposition by alveolar epithelial cells,” *Res. Rep. Biol.*, vol. 2011, no. 2, pp. 1–12, 2011.
- [19] A. Cretu, P. Castagnino, and R. Assoian, “Studying the effects of matrix stiffness on cellular function using acrylamide-based hydrogels,” *J. Vis. Exp.*, no. 42, pp. 7–11, 2010.
- [20] B. Sabass, M. L. Gardel, C. M. Waterman, and U. S. Schwarz, “High resolution traction

- force microscopy based on experimental and computational advances.,” *Biophys. J.*, vol. 94, no. 1, pp. 207–20, 2008.
- [21] J. J. Norman, V. Mukundan, D. Bernstein, and B. L. Pruitt, “Microsystems for biomechanical measurements,” *Pediatr. Res.*, vol. 63, no. 5, pp. 576–583, 2008.
- [22] D. W. Zhou and A. J. Garcia, “Measurement systems for cell adhesive forces,” *J. Biomech. Eng.*, vol. 137, no. 2, p. 20908, 2015.
- [23] J. L. Tan, J. Tien, D. M. Pirone, D. S. Gray, K. Bhadriraju, and C. S. Chen, “Cells lying on a bed of microneedles: an approach to isolate mechanical force.,” *Proc. Natl. Acad. Sci. U. S. A.*, vol. 100, no. 4, pp. 1484–9, 2003.
- [24] C. A. Lemmon, N. J. Sniadecki, S. A. Ruiz, J. L. Tan, L. H. Romer, and C. S. Chen, “Shear Force at the Cell-Matrix Interface: Enhanced Analysis for Microfabricated Post Array Detectors,” *Mech Chem Biosyst*, vol. 2, no. 1, pp. 1–16, 2005.
- [25] M. T. Yang, J. Fu, Y. Wang, R. A. Desai, and C. S. Chen, “Assaying stem cell mechanobiology on microfabricated elastomeric substrates with geometrically modulated rigidity.,” *Nat. Protoc.*, vol. 6, no. 2, pp. 187–213, 2011.
- [26] L. E. Scott, D. B. Mair, J. D. Narang, K. Feleke, and C. A. Lemmon, “Fibronectin fibrillogenesis facilitates mechano-dependent cell spreading, force generation, and nuclear size in human embryonic fibroblasts,” *Integr. Biol.*, vol. 7, no. 11, pp. 1454–1465, 2015.
- [27] K. J. Regehr *et al.*, “Biological implications of polydimethylsiloxane-based microfluidic cell culture,” *Lab Chip*, vol. 9, no. 15, p. 2132, 2009.
- [28] E. J. Hinch, “Lecture Notes Woods Hole GFD Summer School 2003: Introduction to Non-Newtonian Fluids,” vol. 1, no. 5, pp. 1–19, 2003.
- [29] I. D. Johnston, D. K. McCluskey, C. K. L. Tan, and M. C. Tracey, “Mechanical



characterization of bulk Sylgard 184 for microfluidics and microengineering,” *J. Micromechanics Microengineering*, vol. 24, p. 35017, 2014.

## *Thomas John Petet Jr.*

---

(804)-712-0578  
petettj@vcu.edu  
1321 East Main Street  
Richmond, VA 23219

### EDUCATION

---

**Master of Science: Biomedical Engineering**  
*Virginia Commonwealth University, Richmond, Virginia*  
CGPA: 3.00/4.00

September 2014-December 2016

**Bachelor of Science: Biomedical Engineering**  
2014  
*Virginia Commonwealth University, Richmond, Virginia*

- CGPA: 3.02/4.00

September 2011-August

### RESEARCH EXPERIENCE AND AWARDS

---

**Cell and Matrix Mechanobiology Laboratory**  
*Virginia Commonwealth University, Richmond, Virginia*

January 2013 - Present

- Undergraduate research opportunity with Dr. Lemmon from January 2013-August 2014
- Continuation of research as Graduate student with Dr. Lemmon from August 2014 - Present

### WORK EXPERIENCE

---

**Scoutreach Program Aid**  
*Piper Square Community Center, Hopewell, Virginia*

August 2014-August 2016

- Taught scout skills to children in high-risk, low-income environments
- Provided a safe environment to learn about higher education opportunities and help with school work

**After School Team Member**  
*Martial Arts World, Chester, VA*

2006-2007

- Set up a safe environment for youth to complete homework after school as well as train in martial arts

### SKILLS/CERTIFICATIONS

---

#### Technical skills

- MATLAB, Autodesk Inventor, 3D Printing

#### Laboratory skills

- Cell culture, DNA quantification, RNA extraction, microfabrication, BCA protein macro assay, immunosorbent assay, RT-qPCR

## PUBLICATIONS

---

Mair, D. B., Petet, T. J., Scott, L. E., Weinberg, S. H., & Lemmon, C. A. (2015). A Computational Model of Cell-Generated Traction Forces and Fibronectin Assembly. *Biophysical Journal*, 108(2), 471a. <https://doi.org/10.1016/j.bpj.2014.11.2573>